

Opt-in Camera: Person Identification in Video via UWB Localization and Its Application to Opt-in Systems

Matthew Ishige¹, Yasuhiro Yoshimura¹ and Ryo Yonetani¹

Abstract—This paper presents *opt-in camera*, a concept of privacy-preserving camera systems capable of recording only specific individuals in a crowd who explicitly consent to be recorded. Our system utilizes a mobile wireless communication tag attached to personal belongings as proof of opt-in and as a means of localizing tag carriers in video footage. Specifically, the on-ground positions of the wireless tag are first tracked over time using the unscented Kalman filter (UKF). The tag trajectory is then matched against visual tracking results for pedestrians found in videos to identify the tag carrier. Technically, we devise a dedicated trajectory matching technique based on constrained linear optimization, as well as a novel calibration technique that handles wireless tag-camera calibration and hyperparameter tuning for the UKF, which mitigates the non-line-of-sight (NLoS) issue in wireless localization. We realize the proposed opt-in camera system using ultra-wideband (UWB) devices and an off-the-shelf webcam installed in the environment. Experimental results demonstrate that our system can perform opt-in recording of individuals in near real-time at 10 fps, with reliable identification accuracy for a crowd of 8-23 people in a confined space.

I. INTRODUCTION

Cameras are prevalent in a variety of robotics applications, such as mobile robots, social robots, and intelligent surveillance systems. Yet, when it comes to the practical deployment of such camera-equipped robots, privacy and personal data protection pose significant challenges. The EU’s General Data Protection Regulation (GDPR) mandates that business stakeholders obtain valid consent from individuals when processing their personal data, including visual features that can lead to personal identification, specifically for direct marketing applications. Even when not legally required, obtaining informed consent can often be best practice from an ethical perspective, especially in sensitive settings like hospitals and homes.

In this work, we introduce the concept of privacy-preserving camera systems named “*opt-in camera*”, which records individuals in a crowd only when they have explicitly provided their consent to be recorded (*i.e.*, opt-in). As proof of explicit consent, we leverage small wireless communication tags that can be attached to personal belongings. These tags are used to track their carriers via wireless localization techniques [1], and furthermore, to localize them in recorded videos when properly calibrated. For example, consider retail applications. Retailers could provide shopping carts marked “*OK to photograph*”, equipped with wireless tags, alongside regular carts. Opt-in cameras can then track and record only

the individuals carrying the OK-carts, without computationally expensive solutions such as personal identification [2] and re-identification [3].

As the first implementation of the opt-in camera, we develop a system that effectively integrates a surveillance camera and ultra-wideband (UWB) wireless communication devices. Our system performs opt-in recording as follows (see also Fig. 1.) First, on-ground position trajectories of UWB tags are tracked using an unscented Kalman filter (UKF). At the same time, a collection of tracklets for every pedestrian in a video is obtained on the same coordinate system via visual tracking. These tag trajectories and pedestrian tracklets are effectively matched through dedicated constrained linear optimization. To ensure reliable matching even in crowded situations, we develop a novel auto-calibration method that performs wireless tag-camera calibration and hyper-parameter tuning for the UKF from a single pedestrian’s walking demonstration, mitigating the non-line-of-sight (NLoS) issue in UWB-based localization.

We conducted an extensive experiment to evaluate the proposed opt-in camera system. Experimental results demonstrate that our system can successfully identify people in various scenarios, including very crowded ones (see Fig. 5). Our system runs at 10 fps even on consumer laptops (Apple’s M3 Max MacBook Pro), indicating its practical usefulness.

II. RELATED WORK

A. Privacy Protection for Camera Measurement

Ensuring privacy in visual surveillance has been a critical topic in computer vision. A popular approach includes adding noise to recorded videos to make it difficult to identify individuals [4], [5]. Another approach is to use sensors with such low resolution that individuals are difficult to identify to minimize the collection of unnecessary personal information [6], [7]. However, these methods anonymize everyone in the entire image/video, and cannot selectively opt-in or opt-out specific individuals. On the other hand, some prior work aim to identify and track individuals with a wearable cameras [8]–[11]. This line of techniques can allow users to search for themselves in videos recorded by others, and perform post-processing such as masking. Rather than wearable cameras that have their own privacy concerns, our study proposes leveraging UWB-based position estimation to achieve opt-in privacy protection.

B. Indoor Localization with Wireless Communication

Various wireless communication technologies, such as Wi-Fi, Bluetooth, RFID, UWB, have been applied to indoor

¹ M. Ishige, Y. Yoshimura, and R. Yonetani are with Cyber Agent, Inc., Tokyo, Japan {ishige_mashu, yoshimura_yasuhiro, yonetani_ryo}@cyberagent.co.jp

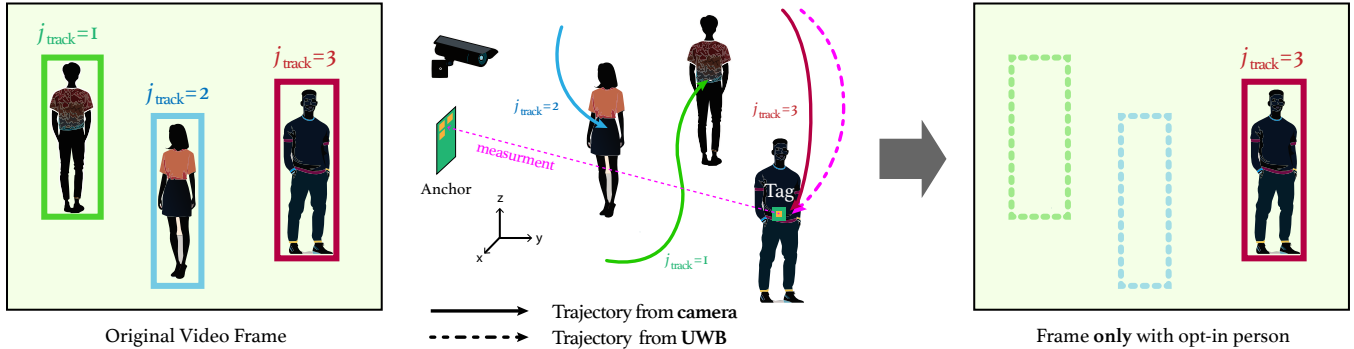


Fig. 1: Overview of opt-in camera.

localization [1], [12]. One of the major technical challenges is the robustness to the non-line-of-sight (NLoS) situations [13] where wireless signals are blocked by environmental obstacles (*e.g.*, furniture and wall) as well as human bodies [14]. Existing work has attempted to mitigate the NLoS in two steps: detecting NLoS moments and mitigating the error (see [13] for a recent survey.) Statistical/learning-based approaches have been taken for NLoS detection [15]–[18], where some work has provided a dedicated benchmark dataset [19], [20]. To alleviate NLoS error, there are not only both learning-based [16], [18], [21]–[23] but also learning-free [24]–[26] approaches that instead assume the availability of measurements from multiple UWB anchors or the prior acquisition of a floor plan. In contrast, we develop a novel auto-calibration method for UWB-based sensing with minimal data collection and labeling, which requires only the walking demonstration of a single pedestrian with a UWB device.

C. Person Identification via Wireless Communication

Finally, there are some existing work trying to identify people/objects in videos using wireless communication technologies. Various methods have been proposed to identify people or objects in videos using wireless communication technologies. The use of RFID systems is popular [27], and more recent work has attempted to integrate deep learning methods in their framework to enable accurate tracking in the 3D space [28], [29]. On the other hand, RFID signals are highly susceptible to environmental factors, requiring environment-specific tuning to maintain the accuracy, where some work has proposed a method specialized to moving objects [30], [31]. Another approach is the use of BLE beacons [32], which could mitigate the NLoS issue by distributing a large collection of beacons in the environment. Compared to these existing studies, our work only requires a single UWB anchor and a UWB tag for every opt-in individual, and can track the individuals even in crowded scenes with significant NLoS effect thanks to novel trajectory matching and auto-calibration techniques.

III. OPT-IN CAMERA SYSTEM

Figure 1 provides an overview of our opt-in camera system. We assume that individuals declare their opt-in for

data recording by carrying small UWB tag devices. Our system identifies those tag-carrying, opt-in individuals in camera footage and mask the other people by replacing their regions with background images. As detailed below, this procedure consists of the following four steps: *UWB-based tracking* to estimate on-ground trajectories of the tag devices (Sec. III-A); *camera-based tracking* to obtain a collection of tracklets for pedestrians shown in a video (Sec. III-B); *trajectory matching* to identify tag carriers in the video (Sec. III-C); and *masking* the video so as to contain the only opt-in individuals (Sec. III-D). Successful identification will require careful calibration of the system in advance, for which we will present a dedicated method in the next section.

A. UWB-based Tracking

Positions of the tags are estimated through wireless communication with a fixed UWB anchor device. This anchor measures the distance and the direction of each tag device as ToF and AoA, first providing tag positions in the polar coordinates centered on the anchor: $\mathbf{z}_t = (z_{\text{radial}}, z_{\text{azimuth}}, z_{\text{polar}})^{\top}$. We then apply an unscented Kalman filter (UKF) [33] to estimate a tag position trajectory $\mathcal{T}^{\text{UWB}} = \mathbf{p}_{0:T}^{\text{UWB}}$ from noisy UWB observations, where $\mathbf{p}_t^{\text{UWB}} = (x, y, z)^{\top}$ represents the tag position in the global Cartesian coordinate system (the magenta dashed curves in Fig. 1). Specifically, the filter tracks a state $\mathbf{s} = (x, v_x, y, v_y, z)^{\top}$ of a tag, where $(v_x, v_y)^{\top}$ represents the on-ground velocities obtained from the UWB measurements $\mathbf{z}_{0:T}$. In practice, there can be multiple individuals with different opt-in UWB tags; let us describe the trajectory for the i -th tag by $\mathcal{T}_i^{\text{UWB}}$.

B. Camera-based Tracking

To the video footage, we apply object detection [34] and multi-object tracking (MOT) [35] algorithms to obtain pedestrian trajectories in the image space, as shown by the solid cyan, green, and red curves in Fig. 1. Our object detection algorithm is customized for humans, allowing us to find bounding boxes not only for the entire body but also for the head region. Assuming that the actual width of human head on average is a constant w_r , the distance (*i.e.*, depth) of the person from the camera can be estimated as $d = f_x \times \frac{w_r}{w_p}$, where f_x is the horizontal focal length of the

camera and w_p is the width of the detected head bounding box. By considering the internal and external parameters of the camera, we can derive the pedestrian tracklets, $\mathcal{T}_j^{\text{cam}}$ for the j -th individual, in the same coordinate system as the tag trajectories obtained in Sec. III-A. Note that multiple tracklets can correspond to a single individual especially when the environment is crowded and people frequently occlude with each other.

C. Trajectory Matching

We match a collection of tag trajectories $\{\mathcal{T}_i^{\text{UWB}}\}$ against that of pedestrian tracklets in a video, $\{\mathcal{T}_j^{\text{cam}}\}$ to identify opt-in tag carriers in the video. We formulate it as a linear assignment problem that assigns a small set of tracklets to each tag trajectory.

Let us introduce a binary assignment matrix $X = (x_{i,j})$:

$$x_{ij} = \begin{cases} 1 & (\mathcal{T}_j^{\text{cam}} \sim \mathcal{T}_i^{\text{UWB}}) \\ 0 & (\mathcal{T}_j^{\text{cam}} \not\sim \mathcal{T}_i^{\text{UWB}}), \end{cases} \quad (1)$$

where $\mathcal{T}_j^{\text{cam}} \sim \mathcal{T}_i^{\text{UWB}}$ means the j -th pedestrian tracklet is a part of the i -th tag trajectory, and $\mathcal{T}_j^{\text{cam}} \not\sim \mathcal{T}_i^{\text{UWB}}$ otherwise. To obtain the matching, we solve the following constrained linear optimization problem:

$$\max_X \sum_{ij} \frac{1}{c_{ij}} x_{ij} \quad (2)$$

$$\text{s.t.} \quad \sum_i x_{ij} \leq 1 \quad (3)$$

$$x_{ij} + x_{i'j} \leq 1 \quad \text{if } \text{duration}(T_j \cap T_{j'}) > s_{\text{slack}} \quad (4)$$

$$x_{ij} = 0 \quad \text{if } c_{ij} > c_{\text{threshold}}. \quad (5)$$

The cost c_{ij} is a time-averaged distance between tag trajectories and pedestrian tracklets:

$$c_{ij} = \frac{1}{|T_i \cap T_j / T_{uc}|} \sum_{t \in T_i \cap T_j / T_{uc}} D(\mathbf{p}_t^i, \mathbf{p}_t^j) \quad (6)$$

where $\mathbf{p}_t^i, \mathbf{p}_t^j$ are the positions of i -th tag and j -th tracklet, and $D(\cdot, \cdot)$ is the Mahalanobis distance based on the covariance matrix of UKF. T_i and T_j are sets of timestamps in $\mathcal{T}_i^{\text{UWB}}$ and $\mathcal{T}_j^{\text{cam}}$, and T_{uc} denotes a set of timestamps where a larger uncertainty is found in tag position tracking, which we detect based on if the largest eigenvalue of the covariance matrix of UKF exceeds a predefined threshold $u_{\text{threshold}}$. The constraint (3) ensures each pedestrian tracklet is assigned to a single tag trajectory, while the constraint (4) prevents simultaneous pedestrian tracklets from being assigned to the same tag trajectory, where overlapping of s_{slack} seconds is allowed for staled tracking IDs in MOT. The constraint (5) eliminates pairs of a tracklet and a trajectory that are too far.

D. Masking

Once we identify pedestrian tracklets matched to tag trajectories, the post-processing for opt-in is straightforward. First, we prepare a clean background image without any person, simply by taking that image when no pedestrians were present or taking average of recording over time. Then we

overlay regions (bounding boxes, or semantic segmentation results if more computation time is allowed) of identified, opt-in individuals onto the image.

IV. SYSTEM CALIBRATION

Our system has several parameters to be determined in advance, including camera intrinsic/extrinsic parameters that can easily be tuned through a standard camera calibration as well as other parameters related to UWB sensing that need to be tuned in a dedicated fashion.

A. Extrinsic Calibration between UWB Anchor and Camera

Matching between UWB tag trajectories and pedestrian tracklets in videos requires the extrinsic calibration between the UWB anchor and the camera, where the key parameters include the position $\mathbf{p}_{\text{anchor}}$ and the antenna direction $\mathbf{r}_{\text{anchor}}$ of the anchor with respect to the camera, as well as the average head width w_r used to convert pedestrian tracklets from image to global coordinate systems.

In this work, we propose a novel calibration method utilizing a demonstration of a single person carrying a tag at a certain height to walk around within the view of the camera. Suppose that we are given a pair of the sequence of UWB data and that of the person's position in video frames. Using the homography transformation matrix derived from anchor position $\mathbf{p}_{\text{anchor}}$ and direction $\mathbf{r}_{\text{anchor}}$, we obtain the tag position $\mathbf{p}_t^{\text{UWB}}$ in the global coordinate system. On the other hand, we also estimate a pedestrian tracklet also in the same global coordinate system using the method in Sec. III-B with parameter w_r , while assuming that the z component (*i.e.*, height) of $\mathbf{p}_t^{\text{cam}}$ to be constant, h_{tag} . We minimize the discrepancy between $\mathbf{p}_t^{\text{UWB}}$ and $\mathbf{p}_t^{\text{cam}}$ over T frames with respect to parameters to be calibrated:

$$\min_{\substack{\mathbf{p}_{\text{anchor}}, \mathbf{r}_{\text{anchor}} \\ w_r, h_{\text{tag}}}} \frac{1}{T} \sum_t \|\mathbf{p}_t^{\text{cam}} - \mathbf{p}_t^{\text{UWB}}\|. \quad (7)$$

We solve this minimization problem through random sample consensus (RANSAC) [36] to alleviate UWB observation noises due to the non-line-of-sight effect explained below.

B. NLoS-aware Parameter Tuning for Kalman Filter

Human bodies, including those of tag carriers, block the line-of-sight (LoS) between UWB tags and the anchor. In such situations, called NLoS, UWB measurements rely on signals propagated through indirect paths, causing substantial localization errors. This effect is especially pronounced in crowded environments, leading to significant localization errors.

In this work, we mitigate this NLoS problem in two steps. First, we learn a binary NLoS detector that identifies NLoS moments from the quality of received signals (*e.g.*, channel impulse responses and signal-to-noise ratios) using the calibration data in the previous section, where samples regarded as outlier in RANSAC (*i.e.*, exceeding a certain error threshold) are labeled as NLoS.

Then, we switch the observation noise covariance matrix R of UKF between NLoS ($R = R_{\text{NLoS}}$) or LoS ($R =$

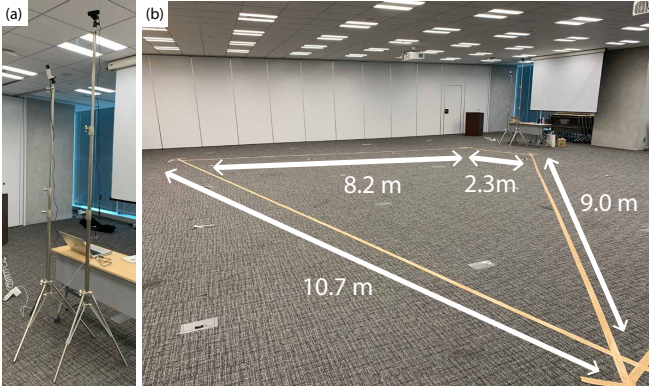


Fig. 2: (a) A UWB anchor device and a camera fixed on tripods. (b) A surveillance area. Subjects randomly walked within this area.

R_{LoS}) based on whether the learned detector $g(\mathbf{f}_t) \in \{0, 1\}$ identifies the current observation as NLoS or not from the signal quality information \mathbf{f}_t .

$$p(\mathbf{s}_t | \mathbf{z}_t) = g_\theta(\mathbf{f}_t) p(\mathbf{s}_t | \mathbf{z}_t; R_{NLoS}) + \{1 - g_\theta(\mathbf{f}_t)\} p(\mathbf{s}_t | \mathbf{z}_t; R_{LoS}). \quad (8)$$

Observation noise covariance matrices R_{NLoS} , R_{LoS} are determined through black-box optimization (CMA-ES [37]) to minimize the largest eigenvalue of the state uncertainty covariance matrix in UKF while constraining estimated tag positions to be within a certain distance of the positions obtained from pedestrian tracklets detected in the video.

V. EVALUATION

We evaluated the tag carrier identification performance of the proposed system from two perspectives: how it performs as the number of individuals in the surveillance area increases and how it performs as the number of opt-in individuals grows. Additionally, we compared the system with a naive baseline to verify the effectiveness of the proposed calibration.

A. Implementation Details

We used the object detection model YOLOv9-Wholebody-with-Wheelchair (C ReLU) from PINTO_model_zoo [38]. For MOT, we used motpy [39]. We obtained the camera parameters using OpenCV’s standard calibration functionality. For the intrinsic parameters, we used a checkerboard pattern. We used an ArUco marker to determine the extrinsic parameters. We trained the NLoS detector using LightGBM [40]. The received signal quality information \mathbf{f}_t was constructed by combining CIR, SNR, RSSI, and the amplitude of peak signals obtained from the anchor antennas. For other parameters, we empirically used the following values: $c_{\text{threshold}} = 2.4$, $u_{\text{threshold}} = 4.0\text{m}$, $s_{\text{slack}} = 0.9\text{s}$. We also used `Q_discrete_white_noise` from filterpy [41] to calculate the process noise in the UKF, with velocity variance set to 4.0 and height variance set to 0.25.

B. Experiment Setups

Hardware: For UWB anchor and tags, we used LBUA0VG2BP-EVK-P and LBUA2ZZ2DK-EVK from Murata Manufacturing Co Ltd. The measurements were available at around 5 Hz for each tag. Detailed device specifications are available on their website [42]. For the surveillance camera, we used a webcam, C920n, from Logitech Co Ltd. We conducted all processing on a consumer laptop from Apple Inc. (MacBook Pro, processor: Apple M3 Max, memory: 64GB). We leveraged the GPUs in the PC to accelerate execution of the object detection.

Field: As for a surveillance area, a trapezoid-like rectangular area was drawn on the floor, and subjects were asked to walk within it randomly. The camera and anchor were set up in front of this area. Both were mounted on tripods and fixed at a height of over 2.0 meters (Fig. 2). As long as standing inside the area, one’s head was visible in the camera.

Baseline Method: Tag positions were estimated using the standard UKF with a fixed observation noise covariance matrix R . We empirically used $R = \text{diag}(0.34, 0.06, 0.04)$ and $w_t = 0.26$. The location panchor and the antenna direction ranchor of the anchor were determined manually. After determining the camera’s extrinsic parameters, we placed an ArUco marker on the floor and used the camera to recognize its position. Then, we placed a tag at the center of the marker to perform UWB positioning, collecting more than ten samples. This process was repeated for three sets, moving the marker for each set. The data obtained were used to determine the installation parameters of the anchor devices.

C. Scalability to the Number of Individuals

We evaluated the identification performance as the number of people in the surveillance area increased. Evaluation data were collected for each condition for 60s and divided into 12 segments, each lasting five seconds. A subject was randomly designated to carry a tag in their right pocket in each condition. We performed trajectory matching for each segment and evaluated the identification accuracy. If the correct individual was identified in more than half of the total frames (*i.e.*, for more than 2.5s), the segment was considered successful.

Figure 3 shows the results. The red line indicates the success rate of the proposed method, while the blue line represents the baseline method. With eight individuals in the area, the proposed method yielded a high success rate. As the number of individuals increased, the success rate declined. When the number reached 23, the success rate fell below 50%. This result is reasonable. As population density increases, MOT becomes more complex, obstructions occur more frequently, and the allowable margin of error for UWB-based tracking decreases as the distance between individuals narrows. On the other hand, the baseline method often failed even in scenarios with fewer individuals, demonstrating the significant effectiveness of the proposed calibration method.

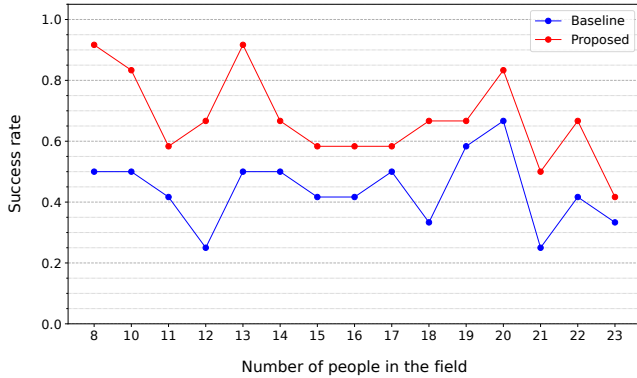


Fig. 3: The identification success rate when there were different numbers of participants in the area.

D. Scalability to the Number of Opt-in Tags

We evaluated identification performance as the number of opt-in individuals (*i.e.*, tags) increased. The total number of individuals in the area was fixed at eight, and the number of tags was increased. The maximum number of tags was set to five. Evaluation data were collected for 60s under each condition and divided into 12 segments, each lasting five seconds. For a given segment, if identification was successful in more than half of the total frames for all tags, the segment was counted as successful.

Figure 4 shows the results. As the red line shows, the proposed method’s success rate declined as the number of opt-in tags increased. However, even with five opt-in tags, more than 66% of the tag carriers were correctly identified. On the other hand, the baseline method had a low identification success rate when there were more than two tags, demonstrating the importance of the proposed calibration.

E. Analysis on Execution Speed

Table I shows a breakdown of the execution time for the opt-in camera system. We present the processing time per video frame. In total, around 50ms was required to process a single frame, meaning the system was able to run at least 10 fps. If the number of individuals in the area increases, the execution time for multi-object tracking increases by 0.08 ms per person. Thus, even if there were 50 people in the area, the increase would only be around 4.0 ms, and it would still be possible to operate at 10 fps. On the other hand, as the number of opt-in individuals increases, the execution time for NLoS detection, the Kalman filter step, and masking also increases. The increase is approximately 2.3 ms per person. Hence, the number of opt-in individuals can be increased to 10 while still running the system at 10 fps. Note that these metrics were obtained from a prototype Python implementation, and implementing in more efficient languages, such as C, may yield better performance.

F. Qualitative Results

Figure 5 shows examples of opt-in camera outcome. It demonstrates the feasibility of the proposed opt-in camera

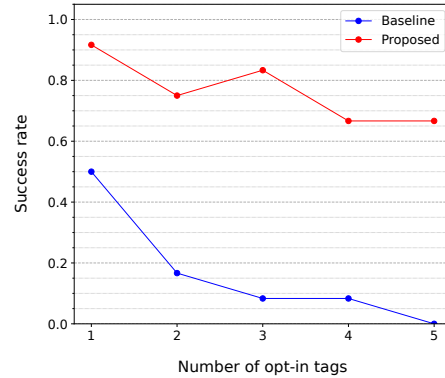


Fig. 4: The identification success rate when there were different numbers of opt-in individuals.

system even in crowded space.

G. Discussion

1) *Reason for the Performance Gap:* We speculate that the adaptive switching of the observation noise covariance matrix is the key factor. Figure 6 presents bird’s-eye views from a single video. (a) and (b) are from the proposed method, while (c) is from the baseline method. The UWB measurement at $t = 4.5$ s (*i.e.*, (b) and (c)) was likely NLoS. As the figure illustrates, the proposed method assigned a large state variance, indicating that it placed less trust in the NLoS observation. In contrast, the baseline method seemed to place trust in the observation, resulting in a significant deviation from the actual position. This difference in handling NLoS observations probably caused the performance gap.

2) *Tuning Threshold Parameters:* $c_{\text{threshold}}$ and $u_{\text{threshold}}$ in (5) control the precision of the identification. Lower values reduce the likelihood of incorrect matches. These parameters should be tuned according to the application’s error tolerance.

3) *Limitations:* The proposed method assumes that object detection and MOT work correctly. However, this assumption may not hold in some cases (e.g., image quality or lighting conditions are poor, population density is very high, and people move rapidly or unpredictably), potentially causing the system to fail. Several approaches could address this issue. For example, depth cameras could make the detection

TABLE I: EXECUTION TIME OF EACH PROCESS IN THE OPT-IN CAMERA SYSTEM.

Name of process	Execution time per frame
object detection	32.28 ± 0.98 ms
multi-object tracking	1.16 ± 0.30 ms
NLoS detection	0.22 ± 0.03 ms
Kalman filter prediction & update	0.60 ± 0.04 ms
tag-image timestamp alignment	1.41 ± 0.18 ms
trajectory matching	1.55 ± 0.09 ms
masking	13.41 ± 0.31 ms
TOTAL	50.63 ms

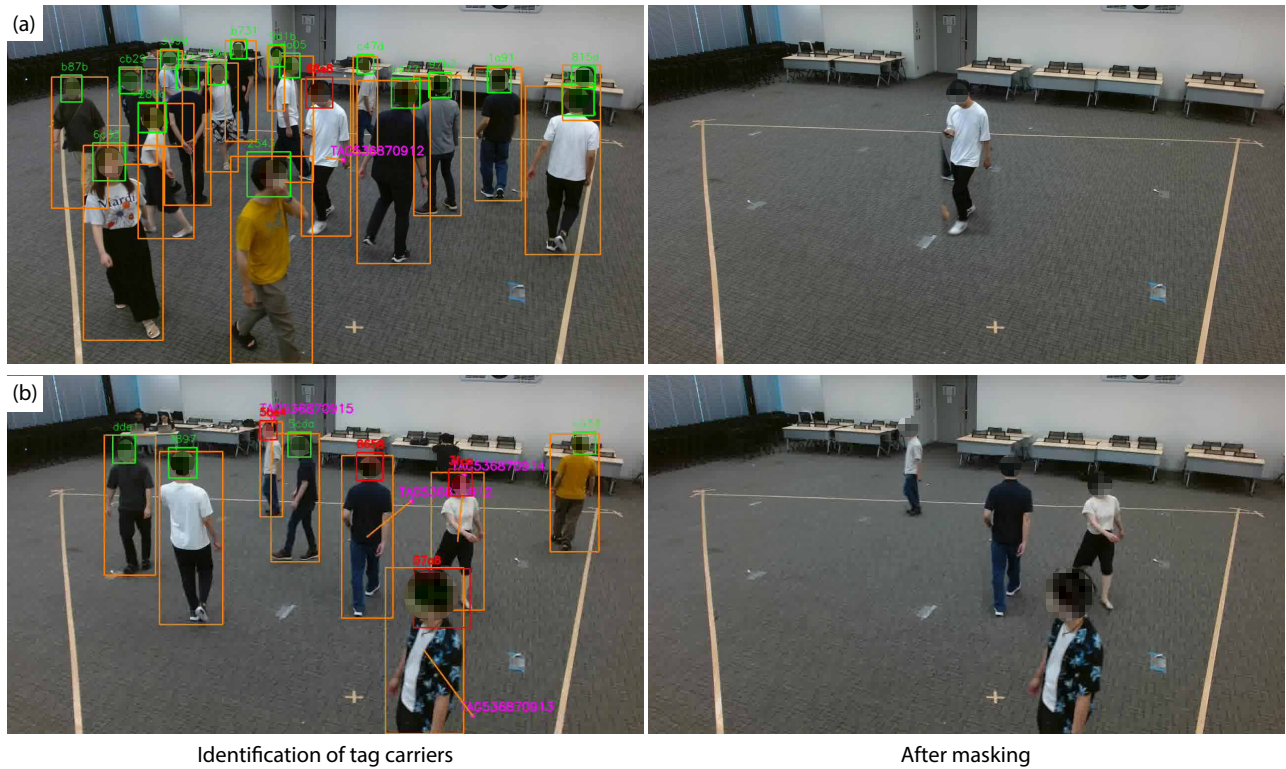


Fig. 5: Visualization of tag carrier identification and masking results. Individuals with red bounding boxes around their heads carried the tags. The estimated locations of the tags are shown as magenta points. The orange lines show associations between the tags and the corresponding carriers’ bounding boxes. Note that a mosaic effect is applied to the facial areas to protect the subjects’ privacy. (a) An example from Sec. V-C. One individual carried a tag among 19 others. (b) An example from Sec. V-D. Four individuals carried tags among four others.

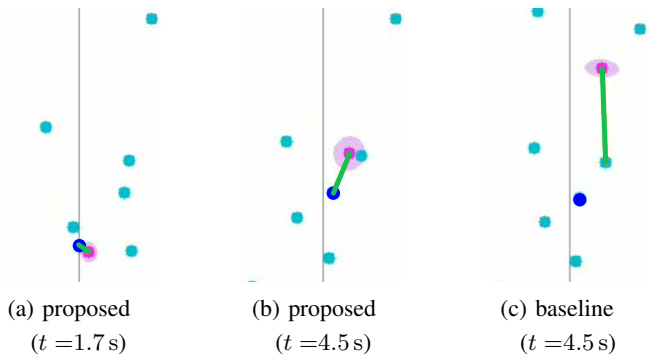


Fig. 6: Bird’s-eye views of scenes from the same video. Cyan dots represent individuals in the area, while blue dots indicate the tag carriers. Magenta dots represent the estimated locations of the tags, with semi-transparent ellipses indicating the square root of the covariance matrix. Green lines show matching results.

more robust, or more advanced MOT methods could handle nonlinear movements. An interesting future direction would be incorporating these approaches into our opt-in camera system.

Another limitation is that the method assumes a fixed camera, like surveillance cameras. This restriction prevents the

introduction of the opt-in camera system into mobile robots. If the camera moves, the naive masking strategy adopted in this study will no longer work effectively. To address this limitation, exploring methods such as in-painting with generative models or leveraging pre-acquired 3D models is an exciting direction for future work.

VI. CONCLUSION

We introduced the concept of an opt-in camera for privacy-preserving sensing and implemented it using UWB-based localization technology. Specifically, individuals who consent to camera recording carry a UWB tag. The system tracks these tags, identifies the corresponding individuals in the video footage, and masks all others, producing a video that captures only opt-in individuals. To mitigate NLoS errors in UWB localization, we proposed a novel calibration method that requires just a few minutes of a pedestrian’s walking demonstration during installation. Extensive evaluation confirmed the system’s effectiveness. We believe this technology addresses privacy concerns and promotes the practical use of camera-based environmental sensing.

REFERENCES

- [1] F. Mazhar, M. G. Khan, and B. Sällberg, “Precise indoor positioning using UWB: A review of methods, algorithms and implementations,” *Wireless Personal Communications*, vol. 97, no. 3, pp. 4467–4491, 2017.

- [2] J. Deng, J. Guo, N. Xue, and S. Zafeiriou, "Arcface: Additive angular margin loss for deep face recognition," in *Proceedings of the IEEE/CVF conference on computer vision and pattern recognition*, 2019, pp. 4690–4699.
- [3] D. Fu, D. Chen, J. Bao, H. Yang, L. Yuan, L. Zhang, H. Li, and D. Chen, "Unsupervised pre-training for person re-identification," in *Proceedings of the IEEE/CVF conference on computer vision and pattern recognition*, 2021, pp. 14 750–14 759.
- [4] Z. Ren, Y. J. Lee, and M. S. Ryoo, "Learning to anonymize faces for privacy preserving action detection," in *Proceedings of the european conference on computer vision (ECCV)*, 2018, pp. 620–636.
- [5] Y. Mi, Z. Zhong, Y. Huang, J. Ji, J. Xu, J. Wang, S. Wang, S. Ding, and S. Zhou, "Privacy-preserving face recognition using trainable feature subtraction," in *Proceedings of the IEEE Conference on Computer Vision and Pattern Recognition (CVPR)*, 2024, pp. 297–307.
- [6] J. Dai, J. Wu, B. Saghafi, J. Konrad, and P. Ishwar, "Towards privacy-preserving activity recognition using extremely low temporal and spatial resolution cameras," in *Proceedings of the IEEE Conference on Computer Vision and Pattern Recognition Workshops (CVPRW)*, 2015, pp. 68–76.
- [7] C. Hinojosa, J. C. Niebles, and H. Arguello, "Learning privacy-preserving optics for human pose estimation," in *Proceedings of the IEEE/CVF international conference on computer vision*, 2021, pp. 2573–2582.
- [8] Y. Poleg, C. Arora, and S. Peleg, "Head motion signatures from egocentric videos," in *Computer Vision—ACCV 2014: 12th Asian Conference on Computer Vision, Singapore, Singapore, November 1-5, 2014, Revised Selected Papers, Part III 12*. Springer, 2015, pp. 315–329.
- [9] R. Yonetani, K. M. Kitani, and Y. Sato, "Ego-surfing first-person videos," in *Proceedings of the IEEE Conference on Computer Vision and Pattern Recognition (CVPR)*, 2015, pp. 5445–5454.
- [10] C. Fan, J. Lee, M. Xu, K. Kumar Singh, Y. Jae Lee, D. J. Crandall, and M. S. Ryoo, "Identifying first-person camera wearers in third-person videos," in *Proceedings of the IEEE Conference on Computer Vision and Pattern Recognition (CVPR)*, 2017, pp. 5125–5133.
- [11] G. A. Sigurdsson, A. Gupta, C. Schmid, A. Farhadi, and K. Alahari, "Actor and observer: Joint modeling of first and third-person videos," in *Proceedings of the IEEE Conference on Computer Vision and Pattern Recognition (CVPR)*, 2018, pp. 7396–7404.
- [12] F. Zafari, A. Gkeliias, and K. K. Leung, "A survey of indoor localization systems and technologies," *IEEE Communications Surveys & Tutorials*, vol. 21, no. 3, pp. 2568–2599, 2019.
- [13] F. Wang, H. Tang, and J. Chen, "Survey on NLOS identification and error mitigation for UWB indoor positioning," *Electronics*, vol. 12, no. 7, p. 1678, 2023.
- [14] A. G. Ferreira, D. Fernandes, S. Branco, A. P. Catarino, and J. L. Monteiro, "Feature selection for real-time NLOS identification and mitigation for body-mounted UWB transceivers," *IEEE Transactions on Instrumentation and Measurement*, vol. 70, pp. 1–10, 2021.
- [15] F. Che, Q. Z. Ahmed, J. Fontaine, B. Van Herbruggen, A. Shahid, E. De Poorter, and P. I. Lazaridis, "Feature-based generalized gaussian distribution method for NLoS detection in ultra-wideband (UWB) indoor positioning system," *IEEE Sensors Journal*, vol. 22, no. 19, pp. 18 726–18 739, 2022.
- [16] H. Yang, Y. Wang, C. K. Seow, M. Sun, M. Si, and L. Huang, "UWB sensor-based indoor LOS/NLOS localization with support vector machine learning," *IEEE Sensors Journal*, vol. 23, no. 3, pp. 2988–3004, 2023.
- [17] Y. Pei, R. Chen, D. Li, X. Xiao, and X. Zheng, "FCN-Attention: A deep learning uwb NLOS/LOS classification algorithm using fully convolution neural network with self-attention mechanism," *Geo-Spatial Information Science*, pp. 1–20, 2023.
- [18] S. Sung, H. Kim, and J. Jung, "Accurate indoor positioning for UWB-based personal devices using deep learning," *IEEE Access*, vol. 11, pp. 20 095–20 113, 2023.
- [19] K. Bregar, A. Hrovat, and M. Mohorcic, "NLOS channel detection with multilayer perceptron in low-rate personal area networks for indoor localization accuracy improvement," in *Proceedings of the 8th Jožef Stefan International Postgraduate School Students' Conference, Ljubljana, Slovenia*, vol. 31, 2016, pp. 1–8.
- [20] V. Barral, C. J. Escudero, J. A. García-Naya, and R. Maneiro-Catoira, "NLOS identification and mitigation using low-cost UWB devices," *Sensors*, vol. 19, no. 16, p. 3464, 2019.
- [21] K. Yu, K. Wen, Y. Li, S. Zhang, and K. Zhang, "A novel NLOS mitigation algorithm for UWB localization in harsh indoor environments," *IEEE Transactions on Vehicular Technology*, vol. 68, no. 1, pp. 686–699, 2018.
- [22] Y. Chen, S. Huang, T. Wu, W. Tsai, C. Liou, and S. Mao, "UWB system for indoor positioning and tracking with arbitrary target orientation, optimal anchor location, and adaptive NLOS mitigation," *IEEE Transactions on Vehicular Technology*, vol. 69, no. 9, pp. 9304–9314, 2020.
- [23] B. Yang, J. Li, Z. Shao, and H. Zhang, "Robust UWB indoor localization for NLOS scenes via learning spatial-temporal features," *IEEE Sensors Journal*, vol. 22, no. 8, pp. 7990–8000, 2022.
- [24] R. Casas, A. Marco, J. Guerrero, and J. Falco, "Robust estimator for non-line-of-sight error mitigation in indoor localization," *EURASIP journal on advances in signal processing*, vol. 2006, pp. 1–8, 2006.
- [25] L. Barbieri, M. Brambilla, A. Trabattori, S. Mervic, and M. Nicoli, "UWB localization in a smart factory: Augmentation methods and experimental assessment," *IEEE Transactions on Instrumentation and Measurement*, vol. 70, pp. 1–18, 2021.
- [26] H. Zhang, Q. Wang, C. Yan, J. Xu, and B. Zhang, "Research on UWB indoor positioning algorithm under the influence of human occlusion and spatial NLOS," *Remote Sensing*, vol. 14, no. 24, p. 6338, 2022.
- [27] C. Duan, W. Shi, F. Dang, and X. Ding, "Enabling rfid-based tracking for multi-objects with visual aids: A calibration-free solution," in *IEEE INFOCOM 2020-IEEE Conference on Computer Communications*. IEEE, 2020, pp. 1281–1290.
- [28] R. Song, Z. Wang, J. Guo, B. S. Han, A. H. Y. Wong, L. Sun, and Z. Lin, "RFID-assisted visual multiple object tracking without using visual appearance and motion," in *2023 IEEE International Conference on Image Processing (ICIP)*. IEEE, 2023, pp. 2745–2749.
- [29] J. Yin, S. Liao, C. Duan, X. Ding, Z. Yang, and Z. Yin, "Robust RFID-based multi-object identification and tracking with visual aids," in *2021 18th Annual IEEE International Conference on Sensing, Communication, and Networking (SECON)*. IEEE, 2021, pp. 1–9.
- [30] Y. Ma, D. Su, Y. Li, C. Tian, and W. Meng, "Spatial perception of tagged cargo using fused RFID and CV data in intelligent storage," *IEEE Internet of Things Journal*, vol. 10, no. 2, pp. 1574–1587, 2022.
- [31] X. Shi, H. Cai, M. Wang, G. Wang, B. Huang, J. Xie, and C. Qian, "Tagattention: Mobile object tracing with zero appearance knowledge by vision-RFID fusion," *IEEE/ACM Transactions on Networking*, vol. 29, no. 2, pp. 890–903, 2021.
- [32] J. Liang, S. Mishra, and C. Wu, "Enhancing person identification for smart cities: Fusion of video surveillance and wearable device data based on machine learning," *IEEE Sensors Journal*, 2024.
- [33] E. A. Wan and R. Van Der Merwe, "The unscented Kalman filter for nonlinear estimation," in *Proceedings of the IEEE 2000 adaptive systems for signal processing, communications, and control symposium (Cat. No. 00EX373)*. IEEE, 2000, pp. 153–158.
- [34] Z. Ge, S. Liu, F. Wang, Z. Li, and J. Sun, "YOLOX: Exceeding YOLO series in 2021," *arXiv preprint arXiv:2107.08430*, 2021.
- [35] A. Bewley, Z. Ge, L. Ott, F. Ramos, and B. Upcroft, "Simple online and realtime tracking," in *2016 IEEE international conference on image processing (ICIP)*. IEEE, 2016, pp. 3464–3468.
- [36] M. A. Fischler and R. C. Bolles, "Random sample consensus: a paradigm for model fitting with applications to image analysis and automated cartography," *Communications of the ACM*, vol. 24, no. 6, pp. 381–395, 1981.
- [37] M. Nomura and M. Shibata, "cmaes: A simple yet practical python library for CMA-ES," *arXiv preprint arXiv:2402.01373*, 2024.
- [38] PINTO0309, "PINTO0309/PINTO_model_zoo," https://github.com/PINTO0309/PINTO_model_zoo, 6 2024, GitHub repository.
- [39] W. Muron, "wmuron/motpy," <https://github.com/wmuron/motpy>, 6 2024, GitHub repository.
- [40] G. Ke, Q. Meng, T. Finley, T. Wang, W. Chen, W. Ma, Q. Ye, and T.-Y. Liu, "LightGBM: A highly efficient gradient boosting decision tree," *Advances in neural information processing systems*, vol. 30, 2017.
- [41] R. Labbe, "FilterPy: Kalman filters and other optimal and non-optimal estimation filters in Python," <https://github.com/rllabbe/filterpy>, 2015.
- [42] Murata Manufacturing Co., Ltd., "my murata," <https://my.murata.com/ja/home>, 2024, Accessed: 2024-09-03.